Vibrational dynamics and structure of graphitic amorphous carbon modeled using an embedded-ring approach

T. E. Doyle
Thiokol Corporation, Brigham City, Utah 84302-0707

J. R. Dennison
Physics Department, Utah State University, Logan, Utah 84322-4415
(Received 31 August 1994)

The Raman spectrum of graphitic amorphous carbon (*g*-C) is modeled with simple classical methods, using rings as medium-range structural units. *g*-C provides a simple [nearly two dimensional (2D) with a single type of atom and one dominant bond type] prototypic example of a large class of continuous random network (CRN) solids where ring or cluster vibrations cannot be decoupled from the network in which they are embedded. We determined the in-plane vibrational modes of $n=4$, 5, 6, 7, and 8-membered symmetric, planar carbon rings using bond-stretching and bond-angle bending force constants; an additional force constant couples each ring node to the surrounding network. Our results support current models of *g*-C as small rafts of nearly 2D CRN's comprised of $\approx 20\%$ $n=5$, 60% $n=6$, and 20% $n=7$ rings, with very few $n=4$ and 8 rings. Extensions of the embedded-ring approach to more complex polyatomic and 3D CRN systems and to other probes of vibrational dynamics are discussed.

INTRODUCTION

A fundamental question in condensed-matter physics is how to progress from our theoretical understanding of crystalline systems with long-range translational order to amorphous systems which lack such ordering. Vibrational dynamics are intimately related to structure and have been used extensively as an indirect probe of the structure of amorphous materials.[1] In an amorphous solid, constituent atoms vibrate about well-defined equilibrium positions, as atoms do in crystals. However, the lack of translational symmetry of the atoms' positions means that Bloch's theorem and the resulting description in terms of phonons used for crystals are not applicable in solving the dynamical equations. A basic understanding of the structure of amorphous materials and their vibrational dynamics at the microscopic level is only now beginning to emerge,[1,2] based on the short- and medium-range order present in both crystalline and amorphous solids.[3]

Most theoretical studies of the vibrational dynamics of amorphous materials take one of two approaches:[1] (1) analytical analysis of small structural units (e.g., tetrahedrally or octahedrally coordinated clusters of atoms) using greatly simplified central-force potential models;[3,4] or (2) numerical methods to calculate vibrational densities of states (VDOS) of large scale cluster models containing many 100's or 1000's of atoms.[1,5] In essence, these methods approach the problem from two limits, by extending short-range atomic (chemical) order or by studying large scale structural models. An intermediate approach developed by Galeener[6] emphasized medium-sized structural elements in the analysis of amorphous solid dynamics. These studies were limited to the analysis of specific vibrational modes in special systems (e.g., rings in SiO_2 (Ref. 6) and B_2O_2-based[7] glasses), which allow ring motion to be entirely decoupled from the surrounding network.[8] Although nearly complete ring-mode decoupling will occur only for a few materials of certain compositions and structures, the use of ring vibrational modes presents a fruitful approach for analytically determining the vibrational characteristics of amorphous materials.

In this paper, we employ a method based on the vibrational dynamics of medium-range structural units (planar rings) which need not be isolated from the surrounding network. A simple method is introduced to couple the rings to the continuous random network (CRN). The modified mode frequencies and the ring statistics are then used to predict theoretical spectra for comparison with real vibrational spectra of materials. We study the vibrational dynamics of two-dimensional (2D) disordered materials by modeling a prototypic, monatomic example of a 2D CRN, graphitic amorphous carbon (*g*-C). *g*-C provides an excellent system for the initial study of our modeling approach as it has been investigated extensively,[9] is approximately 2D in nature, and is not amenable to simple calculations for isolated ring structures since it has only one type of atom and bond (neglecting interlayer π bonds) present. There are two principle goals in this work: (1) to test the validity of our method (the embedded-ring approach) for CRN materials; and (2) to investigate the vibrational dynamics and structural models proposed for *g*-C.

Raman spectroscopy is an appropriate dynamical probe as it is extremely sensitive to both medium- and short-range structural order in *g*-C. Raman spectra of large single-crystal graphite [Fig. 1(a)] exhibits a single high-frequency line (E_{2g} mode) at 1581 cm^{-1}. A breakdown of Raman selection rules allows the A_{1g} mode near

1360 cm^{-1} to become Raman active in nanocrystalline graphite [Fig. 1(b)].[10] Tunistra and Koenig showed the A_{1g}-to-E_{2g} intensity ratio I_D/I_G was inversely related to the intraplanar coherence length L_a of nanocrystalline graphite.[10] The $n=6$ A_{1g} (abbreviated ${}^6A_{1g}$) and similar A_1-type modes are Raman active for isolated rings (see Table I), so the appearance of ${}^6A_{1g}$ in nanocrystalline graphite is not unexpected. The broad, asymmetric Raman spectrum of *g*-C [Fig. 1(d)] is of a commercially available evaporated *a*-C sample which has been well characterized[11] and has a Raman spectrum very similar to other published *g*-C spectra.[12]

THEORY

The embedded-ring approach (ERA) is a generalized, analytical method based upon a common structural unit present in covalent 2D materials—the planar ring.[13] The ERA approach builds upon Galeener's results[6] by expanding upon the use of rings as structural units for vibrational modes and considering the more general case of ring modes coupled to a 2D CRN. The vibrational modes of symmetric, planar *n*-membered rings coupled to an embedding medium and the distribution of ring sizes are used to predict vibrational spectra of CRN materials. These rings are intermediate-sized structural units with 8–18 bonds (more bonds than in a trivalently or tetrahedrally bonded cluster, but many less than in a nanocrystallite or a large cluster of randomly ordered atoms) which reflects the medium-range order present in such materials. The concept combines the methodologies of local dynamics (analytical approaches), the use of mathematical techniques to account for the influence of an embrasive disordered network, and numerical methods (since the vibrational modes of the material are directly computed from the ring statistics of a representative raft model or network cluster).

Vibrational frequencies and modes of oscillations for isolated symmetric, planar rings with $n=4,5,6,7,8$ members were calculated using classical methods of small oscillations[14] for a valence-force model with both a bond-stretching force constant f_r and a bond-angle bending force constant f_Θ. These results were modified by embedding the isolated rings in an effective medium; each atom in the ring was coupled to the surrounding medium through a harmonic coupling force constant f_c which modeled the effect of the embrasive CRN on the ring's vibrational modes (see Fig. 2). Such a coupling scheme is comparable to the use of the cluster-Bethe-lattice method

TABLE I. Frequencies determined with the embedded-ring approach valence-force model.

n	In-plane modes and frequencies (cm^{-1})[a]
4	**A_{1g}(1570), B_{1g}(1350), B_{2g}(1143)**, E_{1u}(709,1584)
5	$A_{1'}$**(1444)**, $E_{1'}$(706,1536), $E_{2'}$**(1100,1529)**
6	**A_{1g}(1360)**, B_{1u}(1455), B_{2u}(1387), E_{1u}(678,1441), **E_{2g}(1010,1569)**
7	$A_{1'}$**(1303)**, $E_{1'}$(653,1371), $E_{2'}$**(945,1531)**, $E_{3'}$(1312,1550)
8	**A_{1g}(1263)**, B_{1g}(1496), B_{2g}(1476), E_{1u}(626,1317), **E_{2g}(896,1471)**, E_{3u}(1220,1572)

[a]Raman-active modes of isolated symmetric rings in bold.

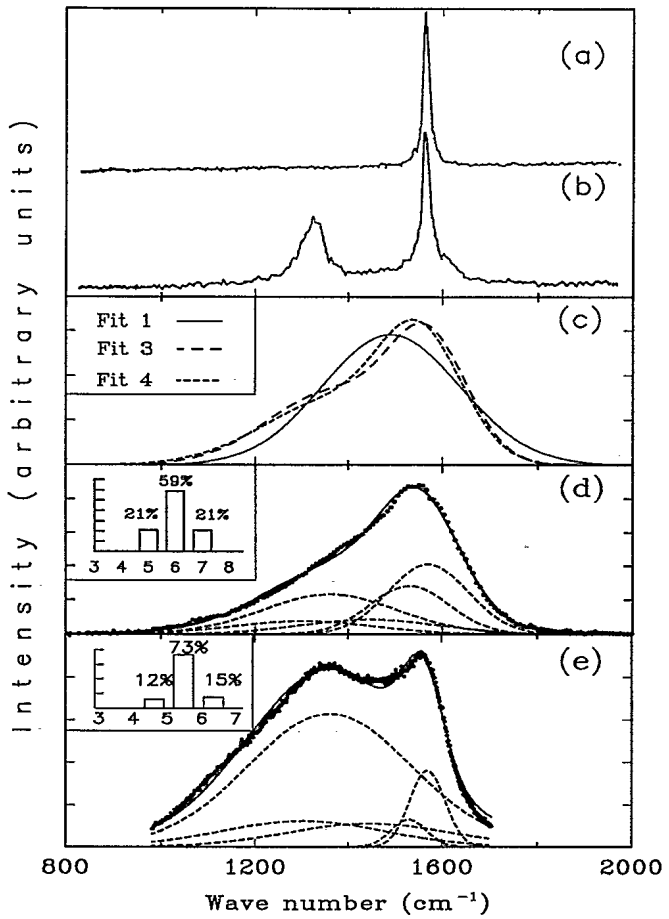

FIG. 1. First-order Raman spectra of (a) graphite, (b) nanocrystalline graphite with $L_a \approx 6$ nm, (d) evaporated graphitic amorphous carbon (*g*-C) (●), and (e) *g*-C annealed at 825 K for ≈40 min (●). (c) Fits to *g*-C Raman spectra as described in Table II. (d) Best fit (Fit 5, Table II) to *g*-C data with Raman-active A_1- and E_2-type $n=5$, 6, and 7 modes. (e) Best fit (Fit 7, Table II) to annealed *g*-C data with Raman active A_1- and E_2-type $n=5$, 6, and 7 modes. Contributions from each component Gaussian peak are also shown [dashed curves in (d) and (e)]. Ring statistics are shown in the insets.

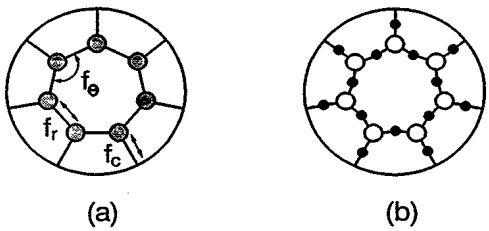

FIG. 2. Structural model for the embedded-ring approach for a 2D amorphous material with (a) monatomic composition and (b) polyatomic (A_2B_3) composition with a triangular cluster on each ring node. The bond-angle bending force constant f_Θ, bond-stretching force constant f_r, and coupling force constant f_c are indicated schematically in (a).

for atoms on cluster surfaces.[1,15] Recently, Galeener *et al.* extended their work on decoupled rings[6] to ring structures in 3D CRN's which were coupled to the surrounding network using a Bethe-lattice method.[16]

Our problem was formulated, in a standard manner used for molecular dynamics, as a secular equation for each vibrational species $\mathbf{V}-\omega^2\mathbf{T}=0$, where $\mathbf{V}$ and $\mathbf{T}$ are the potential and kinetic energy matrices, respectively.[14] The secular equation yielded a $4n\times4n$ secular determinant in terms of the $4n$ generalized coordinates for an n-membered ring. This was factored into smaller secular determinants (2×2 or 4×4 depending on the vibrational species) for each vibrational species by transforming to a set of symmetry coordinates using methods developed by Wilson and co-workers.[14] The factored determinants were solved, the roots of the resulting polynomial equations obtained, and the eigenfrequencies and eigenvectors for each mode of the embedded rings then determined. Details of the methods we used are given elsewhere.[13,17]

The force constants applicable to g-C were determined uniquely by satisfying three constraints based on physical intuition. The secular equations for the Raman-active ${}^6A_{1g}$ and ${}^6E_{2g}$ modes were constrained to match the experimental frequencies (1360 and 1581 cm^{-1}, respectively) of nanocrystalline graphite with a bond length $t=1.42$ Å. In addition, f_c was set equal to $2f_r$. Physically, we expect $f_c\leq2f_r$. In the ${}^6E_{2g}$, ${}^6A_{1g}$, and similar modes, each network atom moves with equal and opposite displacement of the embedded ring atom to which it is coupled (see Fig. 3). The nodes midway between each atom pair, which are present for such motions, can be viewed as a rigid wall coupled to the embedded ring with $f_c=f_r$ and half the ring bond length, or equivalently with unit bond length and $f_c=2f_r$. For other ring motions $f_c<2f_r$. The three constraints then yielded $f_\Theta/t^2=52$ N/m, $f_r=436$ N/m, and $f_c=872$ N/m for g-C with $t=1.46$ Å. These are comparable to values reported in the literature for nearest-neighbor force constants for graphite and sp^2-bonded g-C of $25\leq f_\Theta/t^2\leq267$ N/m (Refs. 5 and 18) and $313\leq f_r\leq459$ N/m.[5,10,18]

Table I shows frequencies calculated from the ERA for all fundamental in-plane modes of the five sizes of rings (this excludes low-frequency rigid translation and rotation A_2-type modes). Figure 3 illustrates the displacement eigenvector diagrams for the A_1-type symmetric breathing modes and E_2-type modes with elongation along an in-plane symmetry axis which are considered in detail below; these six modes are all the $n=5$, 6, and 7 modes which are Raman active for *fully decoupled* symmetric rings.

In principle, there are a large number of adjustable parameters which can be used in fitting the Raman spectrum. However, the frequency, amplitude, and peak shape of each mode for each size ring are, in fact, restricted by the ERA method and other physical arguments. For example, the number of adjustable parameters is the same for two Gaussian fits used by Tunistra and Koenig[10] (two peak positions, two widths and two amplitudes) and the better ERA-based Fits 5 and 7 (ring statistics, ratio of A_1- and E_2-type band proportionality

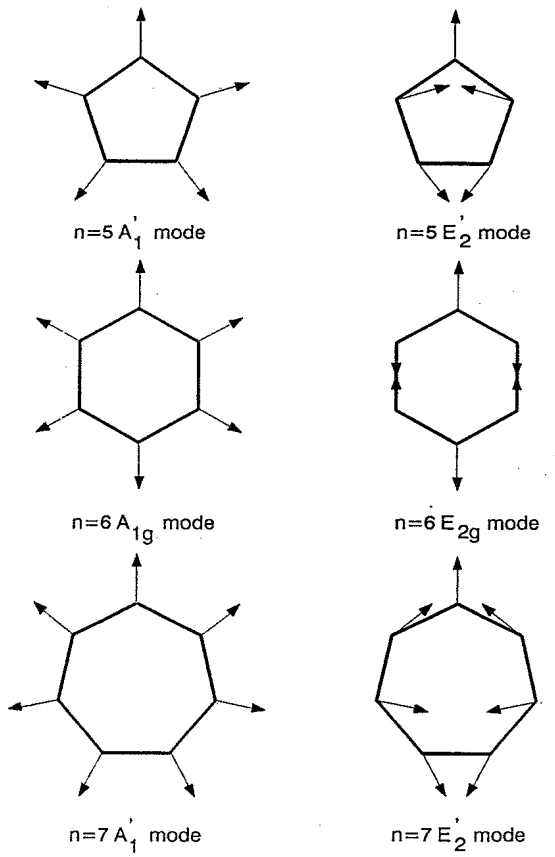

FIG. 3. In-plane A_1- and E_2-type modes of oscillation of embedded rings for the Raman-active modes of isolated 5-, 6-, and 7-membered rings.

constants, band peak widths, and overall intensity), as detailed below. The frequencies used in the fits below are determined uniquely from the ERA calculations after ascertaining the appropriate three force constants. Each mode is modeled as a Gaussian peak profile, in a manner similar to that used in analyzing a-SiO_2 spectra.[19] The width of the peaks is due primarily to the distribution bond angles for asymmetric rings of various sizes and to the sampling of non-zone-center phonons. (We note the potential to model the shape of the broadening function based on a bond-angle distribution directly from ERA calculations.[17]) The amplitude of each model depends on its Raman matrix element in a complicated manner. In addition, modes whose Raman matrix elements are zero may have finite intensities due to breakdown of selection rules (e.g., the ${}^6A_{1g}$ mode discussed above). However, for amorphous, disordered, and liquid materials, the frequency-weighted reduced Raman intensities are approximately constant for modes within a band (e.g., the A_1- or E_2-type modes), and are approximately proportional to the VDOS and hence (in our model) the ring statistics.[12,20] In this approximation, the measured intensity for a given Raman peak is proportional to $I_0N_nc_b\{[n(\omega)+1]/\omega\}$, where I_0 is the incident radiation intensity, N_n are the ring statistics for n-membered rings, c_b is a proportionality constant for band type b, the term in curly brackets is the reduced Raman weighting, and

$n(\omega)=[\exp(\hbar\omega/k_BT)-1]^{-1}$ is the Bose occupation factor.

RESULTS AND DISCUSSION

A series of fits were performed to determine the relative amplitudes and widths associated with the n-membered ring Raman modes.[21] The fitting parameters considered were which modes to include, the overall intensity of the spectra, the ratio c_A/c_E of proportionality constants for A_1-type to E_2-type modes, the ring statistics (with the normalization constraint $\Sigma N_n=1$), and peak widths σ_b for each mode type. The modes considered were, in order, the A_1- and E_2-type Raman-active modes of isolated rings (bold, Table I) for $n=6$, then $n=5$ and 7, and finally $n=4$ and 8; the B-, E_1-, and E_3-Raman-inactive ring modes; and the single Raman-active mode in diamond. The fits used two to six adjustable parameters (bold in Table II). A single Gaussian with variable position, width, and amplitude [Fit 1; Table II and Fig. 1(c)] provided a bench mark to compare with subsequent fits based on calculated Raman peak positions.

Fit 3, which includes the Raman-active $^6A_{1g}$ and $^6E_{2g}$ modes, provides a reasonable fit. This essentially duplicates the result of Dillon, Woollam, and Katkanant who also measured an A_{1g}-to-E_{2g} width ratio σ_D/σ_G of 1.64 for ion-beam and rf-discharge deposited diamondlike amorphous carbon, although their individual widths were 15% larger.[10] Including the $^{5+7}E_{2'}$ modes (Fit 4) further improves the fit; complete ring statistics could not be obtained from this fit since the $^5E_{2'}$ and $^7E_{2'}$ modes are nearly degenerate. The *"best fit"* [Fit 5; Fig. 1(d)] is obtained when all six Raman-active modes are included with ring statistics of 21, 59, and 21 % for $n=5$, 6, and 7, respectively. Addition of neither $n=4$ and 8 Raman-active modes nor Raman-inactive modes significantly improved Fit 5, although it is impossible to preclude small contributions where these peaks overlapped the peaks used in Fit 5. Inclusion of the single Raman-active peak in diamond at 1332 cm^{-1} also did not improve Fit 5, suggesting that sp^3 bonding is not common in g-C. However, the diamond sp^3 Raman cross section is $\sim$50 times smaller than the sp^2 cross section which prohibits detection of small amounts of sp^3 bonding.[5,22]

Peak widths for our g-C fits ranged from 186 to 345 cm^{-1} full width at half maximum (FWHM). These widths are significantly broader than widths found in Raman spectra of water- and fluorine-bearing silica glasses (50–120 cm^{-1} FWHM);[19] this is expected since g-C rings are less isolated from the surrounding network and the 2D nature of the g-C CRN requires a larger bond-angle distribution (estimated as 117°±6° for g-C in Ref. 5) than the 3D silica CRN. We consistently found the width of the A_1-type peaks to be 1.67±0.07 times that for the E_2-type peaks. This may result from enhanced sensitivity of A_1 Kekule-type modes to a bond-angle distribution. The ratio of proportionality constants c_A/c_E remained near unity, as would be expected for bands of modes with similar motion in the same region of the spectrum.

Our results are consistent with previous studies of g-C which suggest that g-C has a nearly 2D CRN structure, formed from 15 to 20 Å diameter nearly planar rafts comprised of $n=5,6,7$ membered rings (with $N_n\approx 21$, 59, and 21 %, respectively), with very few 4- and 8-membered rings, and with little or no sp^3 bonding.[5] Our predicted Raman spectra incorporating Gaussian profile peaks for the Raman-active A_1-type and E_2-type modes for $n=5$, 6, and 7 provided an excellent fit to the measured Raman spectrum of g-C. Also, note that we found $N_5\approx N_7$. Nearly equal numbers of 5- and 7-membered rings are required to minimize puckering (minimal net curvature) of the CRN rafts,[13] since solid-angle deficits created by positive curvature ($n=5$ rings) can be offset by angular excess created by negative curvature ($n=7$ rings).[1] The allowed distribution of 5- and 7-membered rings is severely limited by small puckering observed on amorphous carbon surfaces.[23] Galli *et al.*[24] estimate <1 Å warping locally of the small CRN rafts in g-C.

The Raman spectrum of a thermally annealed g-C sample was also fit to determine the sensitivity of the ERA to structural changes in g-C in terms of ring statistics. Figure 2(e) shows the analysis of a sample annealed *in vaccu* at 825±5 K for $\approx$40 min. The same sequence of fits were performed for the annealed sample as were described above for the g-C sample. Fit 6 used only two Gaussians to fit the data, similar to Fit 3 for g-C and the results of Dillon, Woollam, and Katkanant[10] for annealed diamondlike amorphous carbon and Wada, Gaczi, and Solin[22] for annealed g-C. Fit 6 found a peak intensity ratio $I_D/I_G=8.1$ which corresponds to $L_a\approx 5$ Å using the Tunistra-Koenig relation; such an intraplanar coherence

TABLE II. Fits to Raman spectrum of graphitic amorphous carbon. Variable fitting parameters highlighted in bold.

Fit	Modes included	Ring statistics % $n=\{4,5,6,7,8,9\}$	c_A/c_E	σ_A,σ_E (cm^{-1})	χ^2_{red} [a]
1	single Gaussian $\omega_0=$**1496 cm^{-1}**	100%		$\sigma=$**147**	1.57
2	$^6E_{2g}$	100% $n=6$		$\sigma_E=$**143**	3.48
3	$^6A_{1g}$, $^6E_{2g}$	100% $n=6$	**1.00**	**137,84**	0.67
4	$^6A_{1g}$, $^6E_{2g}$, $^{5+7}E_{2'}$	58% $n=6$, 42% $n=5+7$	**1.04**	**150,86**	0.37
5	$^5A_{1'}$, $^6A_{1g}$, $^7A_{1'}$, $^6E_{2g}$, $^{5+7}E_{2'}$	{0,21,59,21,0}	**1.12**	**146,85**	0.36
6[b]	$A_{1g}(\omega=$**1362 cm^{-1}**$)$, $E_{2g}(\omega=$**1581 cm^{-1}**$)$	100% $n=6$		**179,42**	0.08[b]
7[b]	$^5A_{1'}$, $^6A_{1g}$, $^7A_{1'}$, $^6E_{2g}$, $^{15+7}E_{2'}$	{0,12,73,15,0}	**9.46**	**176,38**	0.07[b]

[a]Refer to Ref. 21 for explanation of reduced chi-squared χ^2_{red}.

[b]g-C sample annealed at 825 K for $\approx$40 min.

length is well below the range for which this relation has been confirmed by comparison to diffraction measurements of the coherence length[10,22,25] and is probably not meaningful. The peak width σ_A was twice that observed by Dillon, Woollam, and Katkanant, while σ_E was approximately the same. Fits using only two peaks (Gaussian, Lorentzian or asymmetric peaks) were not entirely satisfactory, indicating that the standard Tunistra and Koenig analysis, which works well for larger coherence lengths, is insufficient in this case.

Analysis based on ERA results [Fit 7 shown in Fig. 2(e), similar to Fit 5] provides a substantially better fit which predicts 12% $n=5$, 73% $n=6$, and 15% $n=7$ rings, respectively. The initial ERA results for annealed g-C are encouraging (though not definitive) since the fraction of 6-membered rings increases as g-C is annealed, at the expense of $n=5$ and $n=7$ rings, and still maintains $N_5 \approx N_7$. A more complete modeling study of annealed g-C is warranted to systematically investigate trends in the ring statistics.

Our results for g-C and annealed g-C suggest that the ERA has significant potential as a simple method to model the vibrational dynamics of CRN amorphous materials using rings as a medium-range structural unit, particularly in situations that do not allow the rings to be completely decoupled from their surroundings. To test the ERA more thoroughly, we have begun calculations using the ERA to predict the infrared absorption spectrum (which obeys different selection rules than the Raman spectrum) and the inelastic neutron-scattering spectra (which approximates the VDOS) of g-C. Considering the three techniques together, using a consistent structural model (ring statistics), will provide a much more stringent test of the ERA and should further clarify our understanding of the dynamics and structure of g-C.

Other amorphous materials with planar ring structure (e.g., layered materials such as boron nitride, the laminar metal halides, metal dicalcogenides, and certain SiO_2- and B_2O_3-based glasses), and in particular 2D CRN materials of covalent inorganic glasses with binary composition (e.g., As_2Se_3, As_2S_3, As_2O_3, GeO_2, and P_2O_3) can also be studied using this technique. The ERA can also be extended to covalent 3D CRN materials by examining the dynamics of 3D ring structures and polyhedra-forming atomic clusters modified by embedding them in an embrasive network. Such an "embedded polyhedron approach" would have wide application, but more research on the ERA is required before extending the technique to 3D amorphous solids.

ACKNOWLEDGMENTS

We have profited from helpful discussions with Jimmy Ritter, Ron Cappelletti, Bill Kamitakahara, Michael Williams, Mark Holtz, and Jim Wheeler. Mark Holtz, Tim Dallas, and Jeff Wragg provided Raman data for our g-C samples. Support for this work from the USU Office of Research (J.R.D.) is gratefully acknowledged.

[1]S. R. Elliot, *Physics of Amorphous Materials,* 2nd ed. (Wiley, New York, 1990); Nature (London) **354**, 445 (1991).

[2]R. Zallen, *The Physics of Amorphous Solids* (Wiley, New York, 1983).

[3]J. S. Lannin, Phys. Today **41**(7), 28 (1988).

[4]P. N. Sen and M. F. Thorpe, Phys. Rev. B **15**, 4030 (1977).

[5]D. Beeman *et al.*, Phys. Rev. B **30**, 870 (1984).

[6]F. L. Galeener, J. Non-Cryst. Solids **49**, 53 (1982); Solid State Commun. **44**, 1037 (1982); F. L. Galeener *et al.*, Phys. Rev. Lett. **53**, 2429 (1984); S. K. Sharma, J. F. Mammone, and M. F. Nicol, Nature (London) **292**, 140 (1981); S. K. Sharma and B. Simons, Am. Mineral. **66**, 118 (1981).

[7]R. J. Bell *et al.*, J. Non-Cryst. Solids **35&36**, 1185 (1980); C. F. Windisch and W. M. Risen, *ibid.*, **48**, 307 (1982).

[8]F. L. Galeener and M. F. Thorpe, Phys. Rev. B **28**, 5802 (1983).

[9]J. Robertson, Adv. Phys. **35**, 317 (1986).

[10]F. Tunistra and J. L. Koenig, J. Chem. Phys. **53**, 1126 (1970); R. O. Dillon, J. A. Woollam, and V. Katkanant, Phys. Rev. B **29**, 3482 (1984).

[11]J. O. Stoner, Jr., J. Appl. Phys. **40**, 707 (1969); A. L. Ritter, J. R. Dennison, and R. Jones, Phys. Rev. Lett. **53**, 2054 (1984).

[12]J. S. Lannin, Phys. Rev. B **15**, 3863 (1977); N. Wada, J. Non-Cryst. Solids **53**, 543 (1980).

[13]T. E. Doyle, M. S. thesis, Utah State University, 1992.

[14]H. Goldstein, *Classical Mechanics,* 2nd ed. (Addison-Wesley, Reading, MA, 1980), p. 243; E. B. Wilson, Jr., J. C. Decius, and P. C. Cross, *Molecular Vibrations* (Dover, New York, 1955); E. B. Wilson, Phys. Rev. **45**, 706 (1934).

[15]J. D. Jannopoulos, J. Non-Cryst. Solids **32**, 241 (1979).

[16]R. A. Barrio, F. L. Galeener, E. Martinez, and R. J. Elliott, Phys. Rev. B **48**, 15 672 (1993).

[17]T. E. Doyle and J. R. Dennison, Bull. Am. Phys. Soc. **37**(3), 289 (1992); (unpublished).

[18]R. Nicklow, N. Wakabayashi, and H. G. Smith, Phys. Rev. B **5**, 4951 (1972); R. Al-Jishi and G. Dresselhaus, *ibid.* **26**, 4514 (1982); J. A. Young and J. V. Koppel, J. Chem. Phys. **42**, 357 (1965); K. Kesavasamy and N. Krishnamurthy, Ind. J. Pure Appl. Phys. **17**, 73 (1979).

[19]B. O. Mysen and D. Virgo, in *Advances in Materials Research II,* edited by R. L. Snyder, R. A. Condrate, Sr., and P. F. Johnson (Plenum, New York, 1985), p. 43.

[20]R. Shuker and R. W. Gammon, Phys. Rev. Lett. **25**, 222 (1970).

[21]Quality of fit was determined using a minimum distance estimation based on weighted L_2 norms to compare the data to a sum of Gaussian distributions. The sum of the weighted least squares (normally distributed noise with 3–5 % uncertainty) was divided by the number of degrees of freedom to determine if additional fitting parameters signficantly improved the fit. Fitting was performed with a standard analysis package (Sigmaplot, Jandel Scientific) using a Marquardt-Levenberg algorithm. See, e.g., D. M. Titterington, A. F. M. Smith, and U. E. Makov, *Statistical Analysis of Finite Mixture Distributions* (Wiley, New York, 1985), p. 114.

[22]N. Wada, P. J. Gaczi, and S. A. Solin, J. Non-Cryst. Solids **35&36**, 543 (1980).

[23]H.-J. Butt, D. N. Wang, P. K. Hansma, and W. Kuhlbrandt, Ultramicrosc. **36**, 307 (1991); B. Marchon, M. K. Khan, and D. B. Bogy, IEEE Trans. Magn. **27**, 5067 (1991); A. Stemmer *et al.*, Surf. Sci. **181**, 394 (1987); M. Isaacson, J. Langmore, and J. Wall, IITRI/SEM **1974**, 19 (1974).

[24]G. Galli *et al.*, Phys. Rev. Lett. **62**, 555 (1989).

[25]D. S. Knight and W. B. White, J. Mater. Res. **4**, 385 (1989).